Supporting Information for

Effect of Wavelength-Scale Cu_2O Particles on the Performance of Photocathodes for Solar Water Splitting

Jin-Hyun Choi[1], Jehyeok Ryu[1], Hoang Minh Nguyen[2], Jihoon Choi[3], Heeso Noh[3], Seongpil Hwang[2], and Jae-Won Jang[1*]*

[1]Department of Physics, Pukyong National University, Busan 48513, Republic of Korea
[2]Department of Advanced Materials Chemistry, Korea University, Sejong 30019, Republic of Korea
[3]Department of Nano and Electronic Physics, Kookmin University, Seoul, 02707, Republic of Korea

I. Particle size characterization by AFM and XRD measurements

To characterize the particle sizes of the Cu_2O structures, atomic force microscopy (AFM) measurements were carried out. In Figure S1 (a-c), AFM topographic images of the Cu_2O film and Cu_2O patterned structure are displayed. Through grain size analysis in the AFM image processing software (Gwyddion 2.50, Czech Metrology Institute, Czech Republic), the particle sizes of the Cu_2O patterned structure (~ 395 nm and ~ 90 nm) show smaller diameters than those of the Cu_2O film (~ 1260 nm), as shown in Figure S1(d). In addition, the particles at the bottom of the Cu_2O patterned structure (~ 90 nm) are much smaller than those at the top of the Cu_2O patterned structure, which matches the expectation that the growth of the Cu_2O particles is restricted by the reaction space (mold size). The Cu_2O film is obtained without the use of a mold, where Cu freely reacts with the NaOH solution, such that the Cu_2O particles can fully grow (~ 1260 nm). On the other hand, the Cu_2O patterned structure is fabricated with the mold (growth restriction), where the growth of the Cu_2O particles is restricted; hence, the Cu_2O particles cannot fully grow (~ 395 nm). Because the contact region between the Cu layer and the PDMS stamp (the mold) has very limited space between the two surfaces, the growth of the Cu_2O particles is much more restricted such that relatively smaller particles (~ 90 nm) are obtained. The grain sizes (crystalline domains) of the Cu_2O structures can be obtained from the characteristic Cu_2O peaks in the X-ray diffraction (XRD) patterns (Figure S2(a-d)) using the Scherrer equation. By means of the Scherrer equation [1], the grain size (τ) can be calculated as:

$$\tau = \frac{K\lambda}{\beta cos\theta} \qquad (1),$$

where K is a dimensionless shape factor of 0.9, generally[1], λ is the X-ray wavelength (1.54 Å), β is the full width at half maximum (FWHM) of each characteristic peak, and θ is the Bragg angle. In Table S1, the grain sizes of the Cu_2O film and patterned structure are displayed, which were calculated from the Cu_2O characteristic peaks in Figure S2(a-d). Similar to the particle sizes (Figure S1), the grain sizes of the Cu_2O patterned structure are smaller than that of the Cu_2O film.

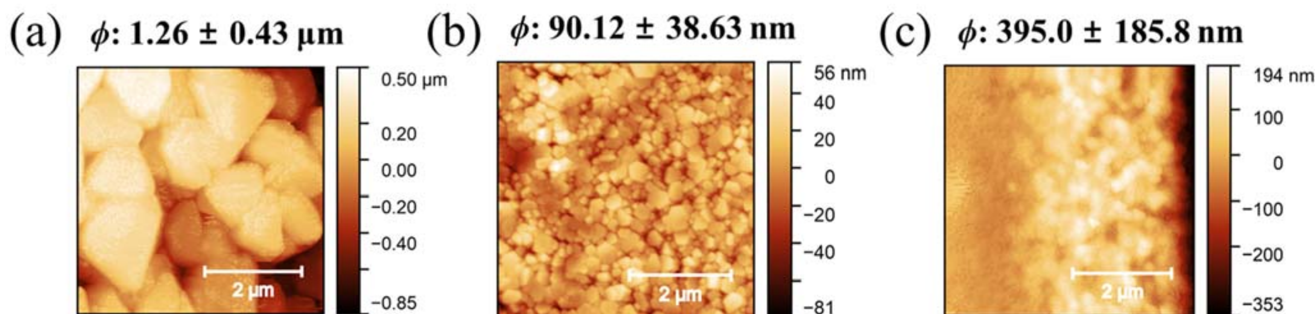

Figure S1 Topological AFM images measured for (a) the Cu_2O film and the (b) bottom and (c) top of the Cu_2O patterned structure. The particle size (ϕ) as analyzed from the AFM images is denoted.

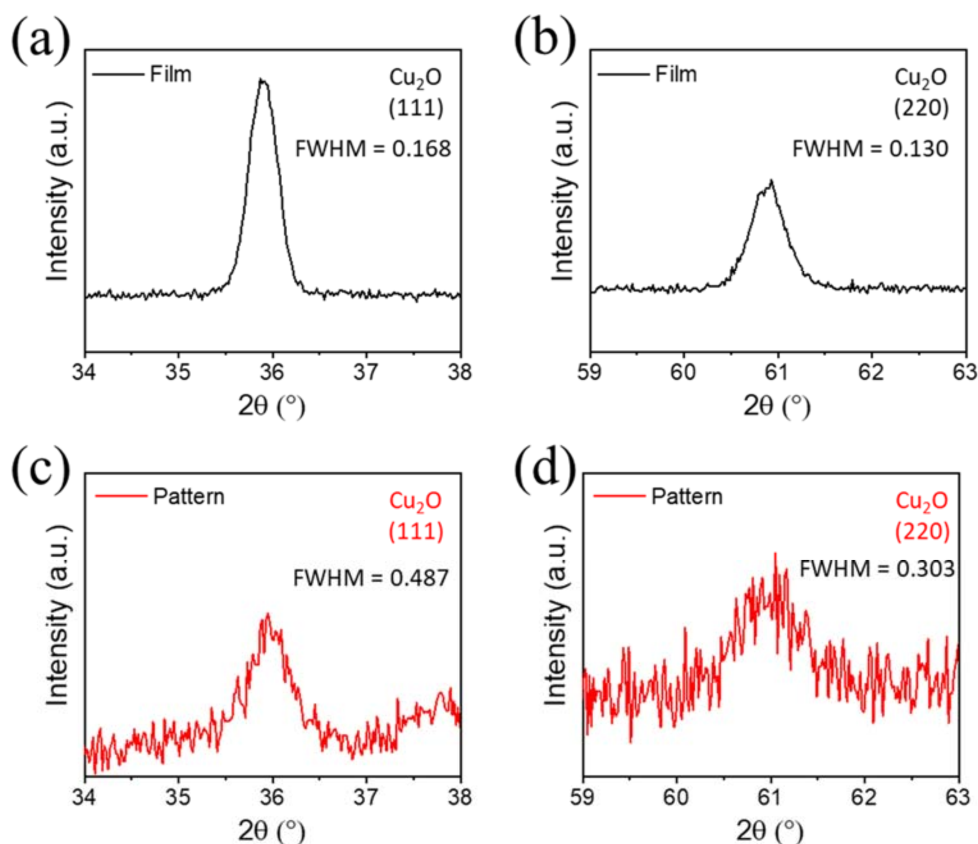

Figure S2 Cu_2O characteristic peaks in the XRD patterns of (a, b) the Cu_2O film and (c, d) the Cu_2O patterned structure. The (a, c) Cu_2O (111) and (b, d) (220) peaks of the film and patterned structure are displayed with their full width at half maximum (FWHM) values.

Grain size of Cu_2O		
Crystalline	**Film**	**Pattern**
(111)	18.05 nm	6.25 nm
(220)	25.84 nm	11.09 nm

Table S1 Grain sizes of the Cu_2O structures obtained from Figure S2 using the Scherrer equation.

II. Cross-sectional SEM measurements of the Cu_2O structures

To compare the thicknesses of the Cu_2O film and patterned structure, cross-sectional SEM images were measured as shown in Figure S3. The thicknesses of the Cu_2O structures can be determined as the distance from the substrate to the top of the Cu_2O structures (denoted as the red arrows in Figure S3). The thickness of the Cu_2O film is approximately 2.6 μm (Figure S3(a)) and that of the Cu_2O patterned structure is approximately 1.3 μm (Figure S3(b)). The different thickness of the Cu_2O film and Cu_2O patterned structure can be explained by Pilling-Bedworth Ratio (PBR). In typical metal oxidation procedure, volume expansion of the metal oxide, compared to the metal volume before the oxidation, is a well-known phenomenon.[2-3] PBR represents the volume change due to oxide formation at the metal and oxide interface. And PBR value of Cu and Cu_2O interface is known about 1.67 (that is the Cu layer can be expanded over 167%).[2] The expended volume ratio of the Cu_2O film and Cu_2O patterned structure can be roughly calculated with the thickness of the final structures, which are 2 – 2.6 (the Cu_2O film) and 1.3 – 1.6 (the Cu_2O pattern), respectively. Figure S3 shows that the fabricated Cu_2O film is not fully filled by the Cu_2O grains while the Cu_2O patterned structure shows the more relatively filled (less empty spaces) structure by the grains. Thus, we assume that the bigger expended volume ratio of the Cu_2O film (2 – 2.6) than the PBR value of Cu and Cu_2O interface (1.67) is reasonable with influences of the empty spaces in the Cu_2O film. Also, the slightly smaller expended volume ratio of the Cu_2O pattern (1.3 – 1.6) than the PBR value of Cu and Cu_2O interface (1.67) can be understood that by the partial transformation of the Cu to Cu_2O happens in the Cu_2O patterned structure.

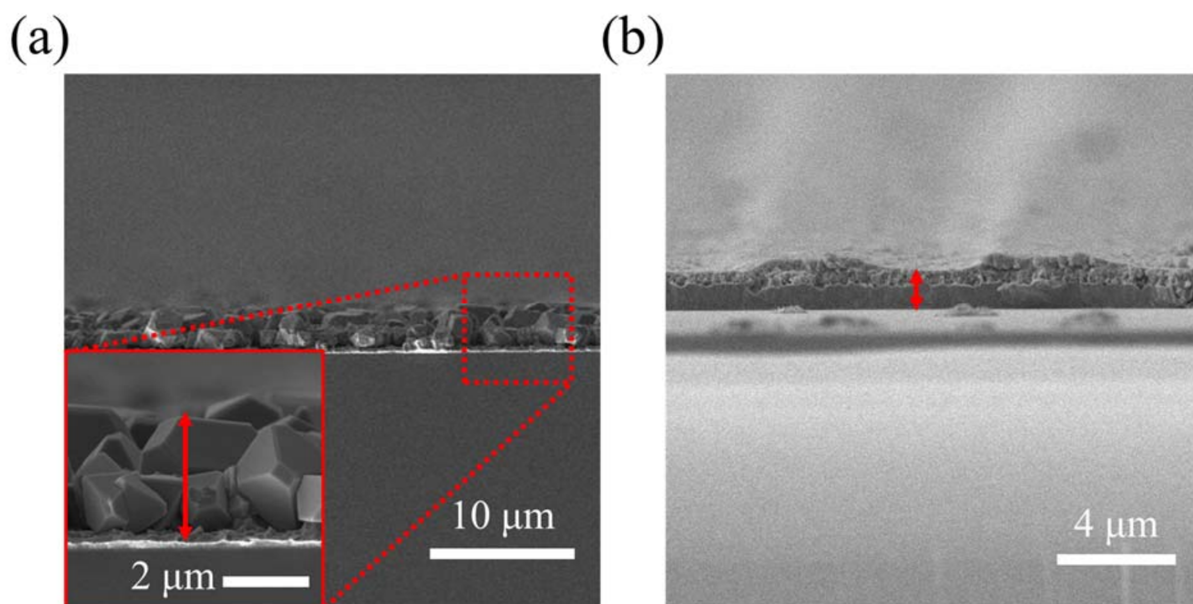

Figure S3 Cross-sectional SEM images of the Cu_2O (a) film and (b) patterned structure. The red double-headed arrows indicate the thicknesses of the structure

III. Detailed setup for the FDTD simulations of the Cu_2O structures

A detailed setup for the FDTD simulations of the Cu_2O structures is shown in Figure S4. A prospective view with labels (the red numbers) for all the components of the FDTD simulations are displayed in Figure S4(a). The FDTD simulations are carried out in a space of 8 μm (x) × 10 μm (y) × 8 μm (z) (displayed as the orange box (“2”)). Periodic boundary conditions (in the x- and z-axes) and perfectly matched layers (PML) (in the y-axis) are used for the FDTD simulations. The plane wave (400 – 900 nm) source is placed 8 μm above (on the y-axis) the bottom of the 50 nm thick Au layer on the glass substrate (“5”). The plane wave proceeds in a direction normal to the Cu_2O structure (“7”). The Cu_2O structure is filled with randomly generated Cu_2O particles. The dimensions of the Cu_2O particles are set to the empirically observed Cu_2O particle sizes (φ_{large}: ~1260 nm, φ_{small}: ~395 nm, Figure S1). The reflection monitor (“3”) and transmission monitor (“4”) are placed 9 μm above and 1 μm below (in the y-axis) the substrate, respectively. Component “6” is a cross-sectional E-field monitor, which is also used as a time-dependent movie monitor. The override mesh region (“8”) is composed of a 10 nm mesh. A cross-sectional view of the Cu_2O structure on the 50 nm thick Au layer on the glass substrate is displayed in Figure S2(b, c). Figure S2(b) and S2(c) correspond to the Cu_2O film and patterned structure, respectively, where the dimensions of the Cu_2O structures are equivalently matched to the empirically measured dimensions of the Cu_2O film and patterned structure (Figure 2).

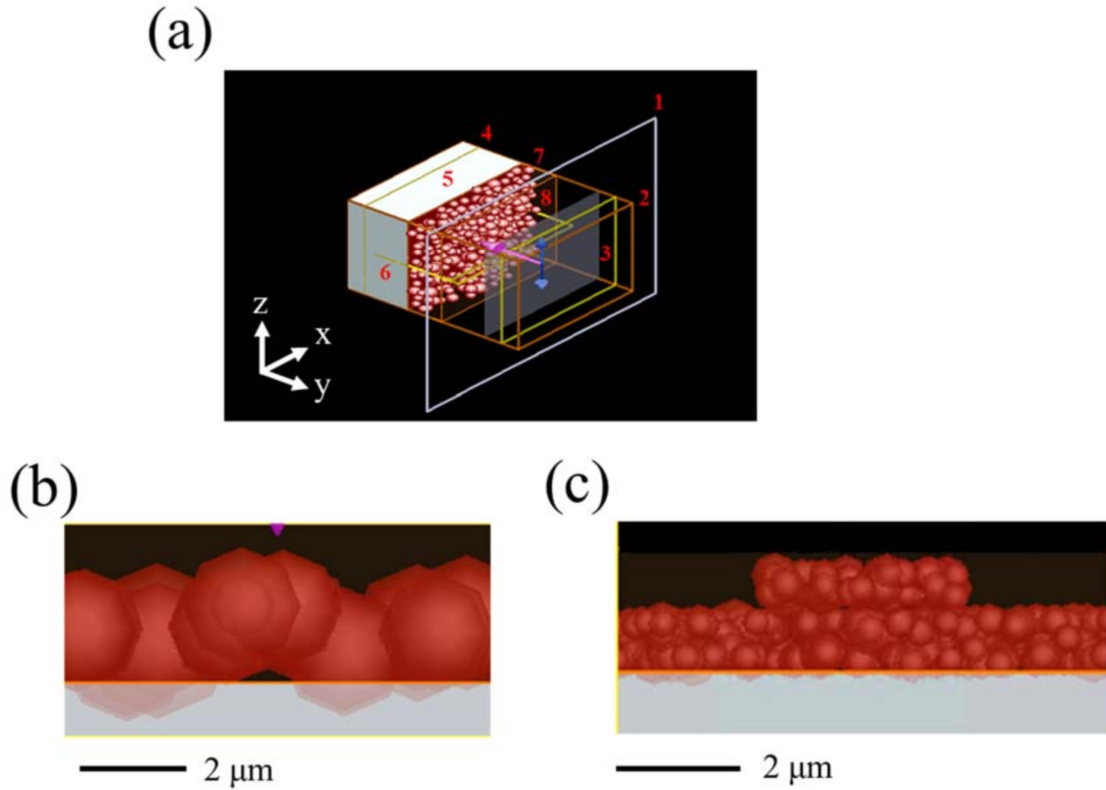

Figure S4 (a) A perspective view of the model used for the FDTD simulations of the Cu_2O samples with x-, y-, z-coordinates. The red-colored numbers are labels for the components (monitors, source, regions, sample object, and region of the override mesh). Cross-sectional view of the Cu_2O (b) film and (c) patterned structure used in the FDTD simulations.

IV. Time-dependent E-field profiles of the Cu_2O structures

Cross-sectional time-dependent E-field profiles were measured as shown in Movie S1. The time at which the incident broadband light source appeared at the top of the monitor is set as the reference time (t = 0 fs). For comparison, E-field profiles with and without the 50-nm-thick Au substrate are measured. In the case of the Cu_2O patterned structure (φ_{small}: ~395 nm), the E-field lasts longer than that in the Cu_2O film (φ_{large}: ~1260 nm). In addition, the E-field lasts longer in the Cu_2O patterned structure with the mirror substrate (50 nm thick Au substrate) than without the mirror substrate. In detail, the lifetimes of the E-field follow the order of the Cu_2O film without the Au substrate (129 fs), the Cu_2O film with the Au substrate (130 fs), the Cu_2O patterned structure without the Au substrate (155 fs), and the Cu_2O patterned structure with the Au substrate (170 fs).

Movie S1 Time-dependent cross-sectional E-field profiles of the Cu_2O film and patterned structure with and without the Au substrate.

V. Thickness dependent absorption of the Cu_2O patterned structure

Finite-difference time-domain (FDTD) simulation is carried out to characterize absorption of equivalently thick Cu_2O film and the Cu_2O patterned structure. Figure S5 shows absorbance spectra of the Cu_2O film (the black line, 2.6 μm thickness), the Cu_2O patterned structure (the red line, 1.3 - 1.6 μm thickness), and the Cu_2O patterned structure of equivalent thickness with the Cu_2O film (the blue line, 2.3 - 2.6 μm thickness) obtained from the FDTD simulations. In Figure S5, the Cu_2O patterned structure of equivalent thickness (the blue box) shows a slightly increasing absorption spectrum than the Cu_2O patterned structure (the red box) without noticeable change of the spectrum. Thus, we conclude that the Cu_2O particle size effect still makes an important role in the absorption of the Cu_2O patterned structure of equivalent thickness. In addition, the slightly increasing absorption of the Cu_2O patterned structure of equivalent thickness (2.3 - 2.6 μm thickness) would result from increasing volume than the Cu_2O patterned structure (1.3 - 1.6 μm thickness), which seems to less influence than the Cu_2O particle size on the absorption.

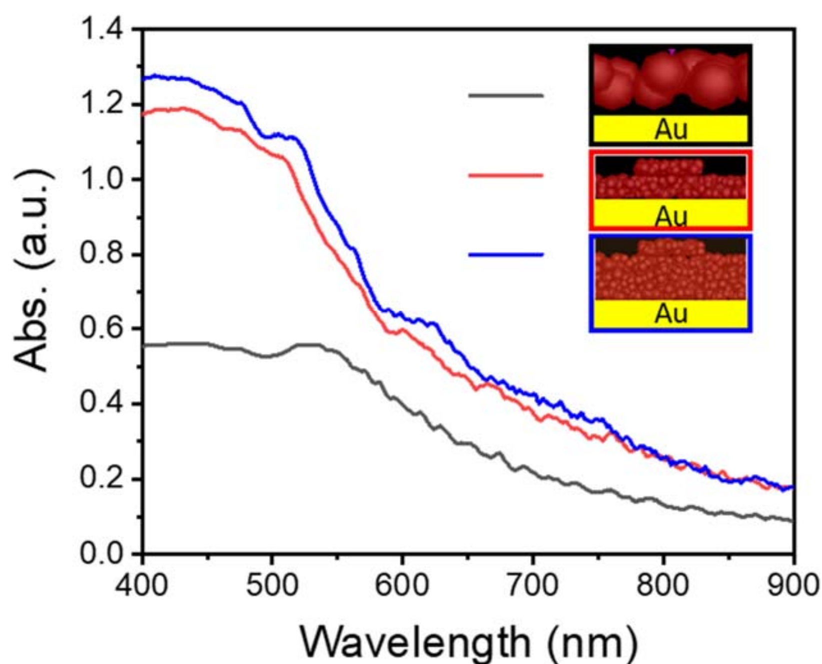

Figure S5. Absorbance spectra of the Cu_2O film (the black box), the Cu_2O patterned structure (the red box), and the Cu_2O patterned structure of equivalent thickness with the Cu_2O film (the blue box obtained from the FDTD simulations.

VI. Photoluminescence spectra and time-resolved photoluminescence parameters of the Cu_2O photocathodes

Photoluminescence (PL) spectra of the Cu_2O photocathodes are presented in Figure S6. Y1 exciton peak (~ 635 nm) of the Cu_2O[4-5] is observed both in the Cu_2O film and pattern photocathodes. The PL decay curves, which are presented in Figure 5(c) and 5(d) in the manuscript, are fitted with Eq. (3) in the manuscript. Parameters obtained from the fitting are presented in Table S2.

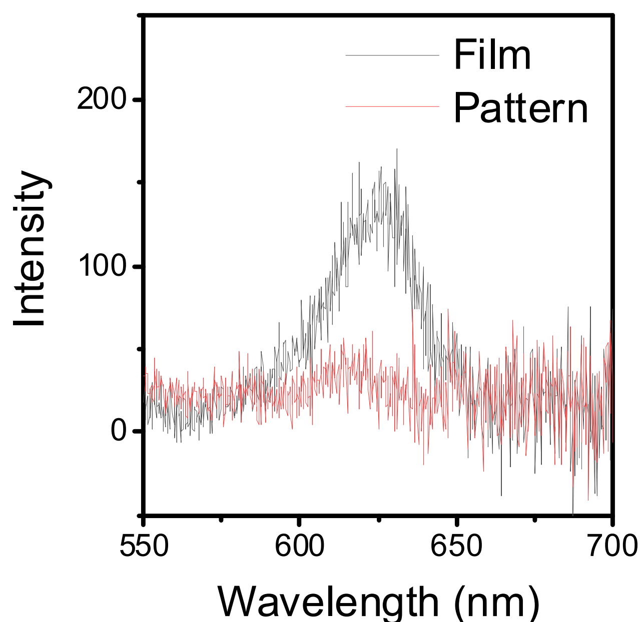

Figure S6. PL spectra of the Cu_2O film and the Cu_2O pattern photocathodes.

	A_1	τ_1 (ns)	A_2	τ_2 (ns)
Film	3924.7	0.226 ± 0.002	433.1	0.709 ± 0.027
Pattern	186.0	0.167 ± 0.001	35.9	0.538 ± 0.064

Table S2. Parameters of the PL decay of the Cu_2O photocathodes fitting with Eq. (3) in the manuscript.

VII. Cu_2O patterned structure fabricated by Au nanomembrane-based lithography

According to our previous report on Au nanomembrane-based lithography[6], a thin Au film (nanomembrane) on top of the reacting metal layer (in our case, the Cu layer) is beneficial for the fabrication of a more uniform molded structure. Hence, a Cu_2O patterned structure was also fabricated using Au nanomembrane-based lithography. The fabrication method for Au nanomembrane-based lithography is the same as the method shown in Figure 1, except for the deposition of a Au nanomembrane (20 nm) on the Cu/Au/Ti (1000/50/10 nm) film on the glass substrate. The AFM measurements of the Cu_2O patterned structure fabricated using Au nanomembrane-based lithography are shown in Figure S5(a, b). The fabricated Cu_2O structure has a more distinct patterned structure (but the height of the pattern is smaller) than the Cu_2O patterned structure shown in Figure 2 and Figure S1(b, c). The magnified image in Figure S5(a) was used for particle size analysis. The particle size of the Cu_2O patterned structure fabricated using Au nanomembrane-based lithography is 63 ± 19 nm (measured at the top of the pattern), which is smaller than the top of the Cu_2O patterned structure prepared without lithography (particle size: ~395 nm), as shown in Figures 2 and S1. The height of the Cu_2O patterned structure fabricated using Au nanomembrane-based lithography is approximately 40 nm, as shown in Figure S5(b).

In addition, the photocatalytic activity of the Cu_2O patterned structure fabricated using Au nanomembrane-based lithography is characterized by photoelectrochemistry (PEC) measurements with the light on and off. As shown in Figure S5(c), no distinct photocurrent density can be observed. We assume that the Cu_2O structure is too thin to work as a light absorber and does not necessarily work during the PEC process, where the lower Au nanomembrane can directly react with the ions in the solution.

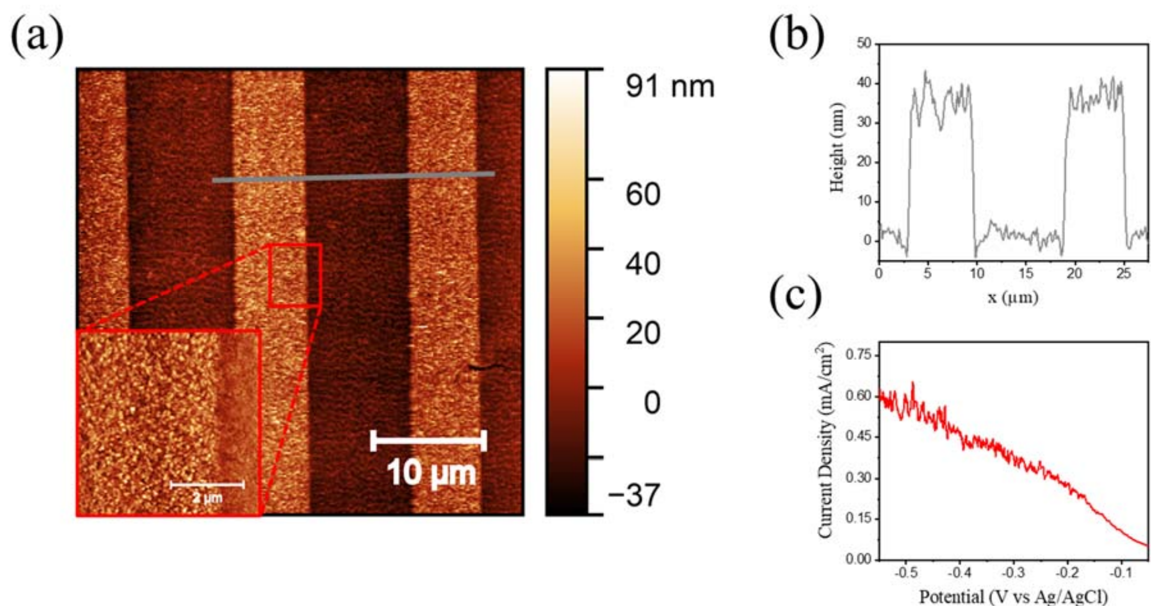

Figure S7 (a) A topological AFM image of a Cu_2O patterned structure fabricated using Au nanomembrane-based lithography. The inset is a magnified image of the region observed in the red box. (b) A cross-sectional line profile (obtained from the dark gray line in (a)). (c) Potential-dependent current density curve of the Cu_2O patterned structure fabricated using Au nanomembrane-based lithography obtained from the PEC measurements.

VIII. Photostability of the Cu_2O photocathodes

To test the photostability of the Cu_2O photocathodes, we measured time-dependent photocurrent density of the Cu_2O film and the Cu_2O pattern photocathodes (PEC measurement at -0.4 V *vs.* Ag/AgCl). Figure S8 are the same data as the inset of Figure 5(b) in the manuscript. Figure S8 is differently displayed in min- and sec-scales to emphasize the saturated time of photocurrent densities. Figure S8(a) and S8(b) show that photocurrent density of the Cu_2O patterned structure becomes stable (~ 50 sec, the red-line in Figure S8(a)) faster than the Cu_2O film (~ 50 min, the black-line in Figure S8(b)). The faster time of the Cu_2O patterned structure to be photostable would be related to the better durability of the Cu_2O patterned structure than that of the Cu_2O film. (mentioned in the manuscript with the lower onset potential of the Cu_2O patterned structure).

In addition, to verify the reproducibility of the Cu_2O photocathodes, reproducible PEC activity of the Cu_2O photocathodes for different LSV scans was evaluated with dark and light irradiated current densities measured before and after the photostability test of the Cu_2O photocathodes (the hour-scale time-dependent photocurrent densities (J_{Ph}-t) shown in Figure S8(a)). Figure S8(a) shows the dark and light irradiated current densities LSV measurements of the Cu_2O film photocathode; the solid lines (same data shown in Figure S8(a)) and the dotted lines represent the data obtained before and after the 5 hours continuing photostability test, respectively. The current densities measured after the photostability test somehow decrease, and on-set potential of anodic photocurrent (the crossover potential of the dark and light irradiated current densities) negatively increases (from ~ -1V to ~ -0.15 V). On the other hands, the dark and light irradiated current densities LSV measurements of the Cu_2O pattern photocathode are displayed in Figure S8(b); the solid lines (same data shown in Figure S8(b)) and the dotted lines represent the data obtained before and after the 10 hours continuing photostability test, respectively. It turns out that both Cu_2O film and pattern photocathodes are degraded after long exposure of the light irradiation, but the on-set potentials of the anodic photocurrent in the Cu_2O film are expected to be more negative (See the crossover points of the dark and light irradiated current densities), which was reproducibly observed in Figure 5(b) of the manuscript. To further investigation, we obtain photocurrent densities of the Cu_2O photocathodes from Figure S8 (a) and (b) (by subtracting the dark current densities to the light irradiated current densities) and display in Figure S8 (c) and (d). Despite photo-degradations, the photocurrent densities of the Cu_2O pattern photocathode are still higher than the Cu_2O film photocathode. Therefore, it can be concluded that the PEC activity of the Cu_2O photocathodes is reproducible

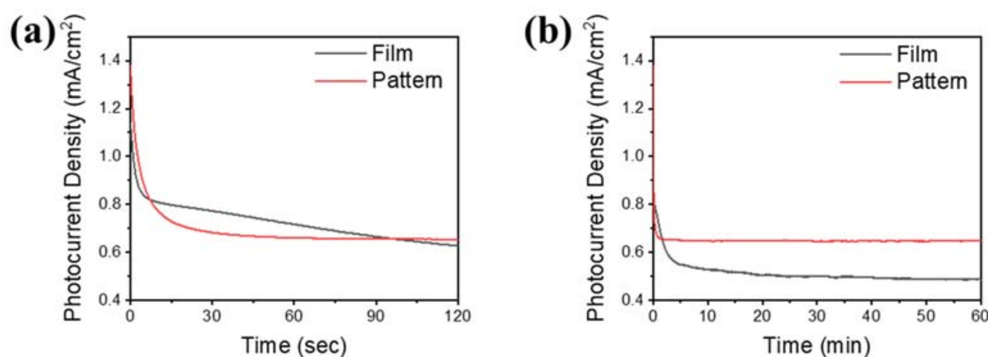

Figure S8. Time-dependent photocurrent density of the Cu_2O film and the Cu_2O pattern photocathodes in (a) sec- and (b) min-scales. The photocurrent densities are measured with PEC set-up (at -0.4 V vs. Ag/AgCl with 1.5 AM halogen lamp).

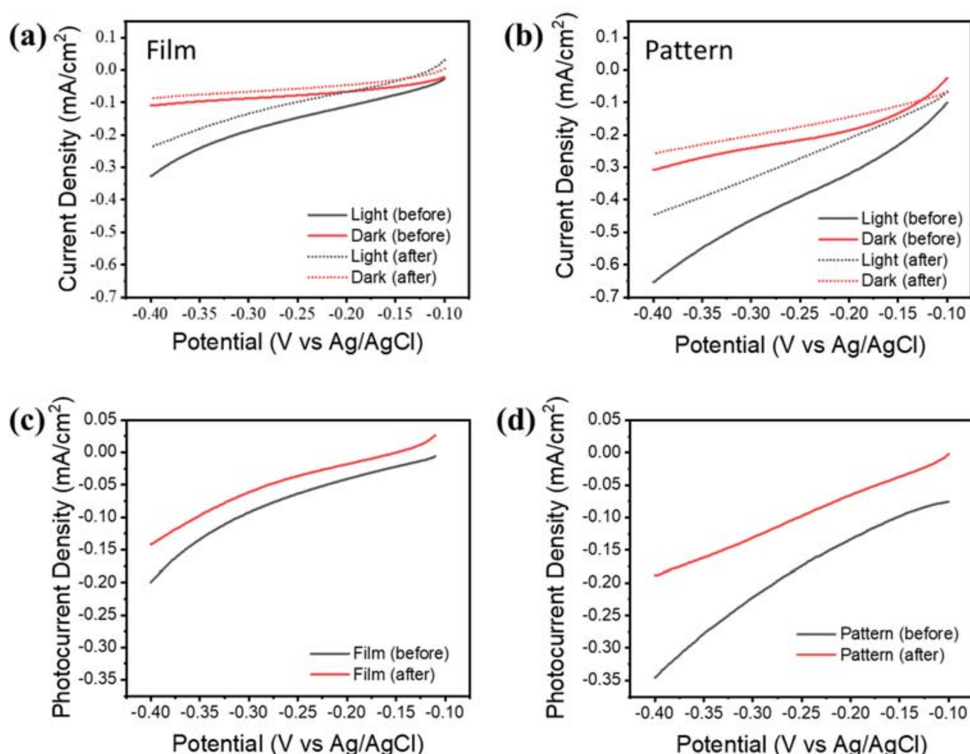

Figure S9. (a) Dark and light irradiated current densities LSV measurements of the Cu_2O film photocathode, obtained before (the solid lines) and after (the dotted lines) 5 hours continuing time-dependent photocurrent density (J_{Ph}-t) measurements. (b) Dark and light irradiated current densities LSV measurements of the Cu_2O pattern photocathode, obtained before (the solid lines) and after (the dotted lines) 10 hours continuing J_{Ph}-t measurements. (c,d) The photocurrent densities of the Cu_2O photocathodes obtained from before (the black lines) and after (the red lines) the J_{Ph}-t measurements. (c) and (d) are obtained from (a) and (b), respectively.

References

[1] Monshi, A.; Foroughi, M. R.; Monshi, M. R. Modified Scherrer Equation to Estimate More Accurately Nano-Crystallite Size Using XRD. *World J. Nano Sci. Eng.* **2012**, *2*, 7.

[2] German, R. M.; Munir, Z. A. A Correlation between the Pilling-Bedworth Ratio and the Radius of Curvature of Metallic Substrates with Coherent Thin Oxide Layers. *Oxid. Met.* **1974**, *8*, 123-129.

[3] Xu, C.; Gao, W. Pilling-Bedworth Ratio for Oxidation of Alloys. *Mater. Res. Innov.* **2000**, *3*, 231-235.

[4] Wang, P.; Zhao, X.; Li, H.; Li, L.; Li, J.; Ma, G.; Chang, J. Temperature Sensitive Optical Properties of Exciton and Room-Temperature Visible Light Emission from Disordered Cu_2O Nanowires. *RSC Adv.* **2014**, *4*, 37542-37546.

[5] Hossain, M. A.; Al-Gaashani, R.; Hamoudi, H.; Al Marri, M. J.; Hussein, I. A.; Belaidi, A.; Merzougui, B. A.; Alharbi, F. H.; Tabet, N. Controlled Growth of Cu_2O Thin Films by Electrodeposition Approach. *Mat. Sci. Semicon. Proc.* **2017**, *63*, 203-211.

[6] Oh, C.-M.; Park, K. H.; Choi, J.-H.; Hwang, S.; Noh, H.; Yu, Y. M.; Jang, J.-W. Polycrystalline Au Nanomembrane as a Tool for Two-Tone Micro/Nanolithography. *Chem. Mater.* **2017**, *29*, 3863-3872.